Ann. Geophysicae 12, 664–673 (1994)

Annales Geophysicae

Theoretical validation of ground-based microwave ozone observations

P. Ricaud[1], G. Brasseur[2], J. Brillet[1], J. de La Noë[1], J.-P. Parisot[1], M. Pirre[3]

[1] Bordeaux Observatory, BP 89, F-33270, Floirac, France
[2] NCAR*, PO Box 3000, Boulder, CO 80307, USA
[3] LPCE, 4A Avenue de la Recherche Scientifique, F-45071, Orléans Cedex, France

Received: 21 October 1993/Revised: 9 February 1994/Accepted: 21 February 1994

Abstract. Ground-based microwave measurements of the diurnal and seasonal variations of ozone at 42 ± 4.5 and 55 ± 8 km are validated by comparing with results from a zero-dimensional photochemical model and a two-dimensional (2D) chemical/radiative/dynamical model, respectively. O_3 diurnal amplitudes measured in Bordeaux are shown to be in agreement with theory to within 5%. For the seasonal analysis of O_3 variation, at 42 ± 4.5 km, the 2D model underestimates the yearly averaged ozone concentration compared with the measurements. A double maximum oscillation ($\sim 3.5\%$) is measured in Bordeaux with an extended maximum in September and a maximum in February, whilst the 2D model predicts only a single large maximum (17%) in August and a pronounced minimum in January. Evidence suggests that dynamical transport causes the winter O_3 maximum by propagation of planetary waves, phenomena which are not explicitly reproduced by the 2D model. At 55 ± 8 km, the modeled yearly averaged O_3 concentration is in very good agreement with the measured yearly average. A strong annual oscillation is both measured and modeled with differences in the amplitude shown to be exclusively linked to temperature fields.

1 Introduction

Ground-based microwave observations have been carried out intensively over the last 10 years to study the short- and long-term behavior of atmospheric trace gases. Examples include: water vapor seasonal variations by Bevilacqua *et al.* (1990), ozone diurnal variations by Wilson and Schwartz (1981), ozone seasonal variations by Connor *et al.* (1987), and chlorine monoxide diurnal variations by De Zafra *et al.* (1989). The comparison of data with models is a crucial indicator of our knowledge about the dynamical, chemical and radiative processes which occur in the middle atmosphere (see e.g., in the microwave range, Zommerfelds *et al.* (1989) for ozone, Bevilacqua *et al.* (1990) for water vapor and Solomon *et al.* (1984) for chlorine monoxide). The most obvious problem when attempting to interpret ground-based microwave measurements is that their vertical resolving power is limited to 5 km (see Bevilacqua and Olivero, 1988). Direct comparison with models whose vertical resolution is usually better than the resolving power of the instrument has thus to be made with great care.

Diurnal and seasonal variations of O_3 concentrations measured in Bordeaux, France from September 1985 to October 1990 at 42 ± 4.5 and 55 ± 8 km by means of a ground-based microwave receiver have already been reported in Ricaud *et al.* (1991). The aim of this paper is to validate the measured diurnal variations by comparison with a zero-dimensional (0D) photochemical model and to validate the measured seasonal variations by comparison with the two-dimensional (2D) chemical/radiative/dynamical model of Brasseur *et al.* (1990). The validation phase will take into account the poor height-resolving power of the ground-based microwave measurements by processing the modeled O_3 vertical profile $\varrho(h)$ as (see Ricaud *et al.*, 1991)

$$\langle \varrho(h_0) \rangle = \int_0^H \frac{s(h, h_0) \varrho_0(h_0)}{\varrho_0(h)} \varrho(h)\, dh, \tag{1}$$

where $H = 90$ km, $\varrho_0(h)$ is a standard ozone profile taken from Brillet (1989), $s(h, h_0)$ is the scanning function derived from the Backus and Gilbert (1970) inversion theory and now $\langle \varrho(h_0) \rangle$ is the O_3 concentration modeled at 42 ± 4.5 and 55 ± 8 km for $h_0 = 42$ and 55 km, respectively.

Section 2 deals with O_3 diurnal variations. The time-dependent 0D model used in this study is presented and measured variations are compared with the modeled ones. Section 3 discusses O_3 seasonal variations. The 2D model used in this study is briefly presented and finally, measured seasonal variations are compared with modeled ones.

Correspondence to: P. Ricaud
*The National Center for Atmospheric Research is sponsored by the National Science Foundation

2 Ozone diurnal variations

2.1 The 0D model

The model used in the analysis of the diurnal variations of ozone measured in Bordeaux is a time-dependent 0D model including 20 species belonging to the odd oxygen (O_3, $O(^1D)$, $O(^3P)$), odd hydrogen (H, OH, HO_2, H_2O_2, CH_3O_2), odd nitrogen (N, NO, NO_2, NO_3, N_2O_5, HNO_3, HO_2NO_2), and odd chlorine (Cl, ClO, HCl, HOCl, $ClONO_2$) families. Total odd nitrogen and total odd chlorine are implicitly set by their initial condition values. The concentrations of long-lived gases which exhibit no significant diurnal variation (H_2O, H_2, CH_4, N_2O, CFCs, CO) are specified. Transport is ignored. All altitude levels are radiatively coupled by the computation at each time step of the ozone column abundance and the use of the multiple scattering method of Meier *et al.* (1982) for the calculation of the photolysis rates. Since in the upper stratosphere and in the mesosphere the photochemical time constant of ozone is much smaller than its dynamical time constant (see Brasseur and Solomon, 1984), ozone can be assumed to be in photochemical equilibrium and a 0D chemical model is adequate to describe the diurnal variation of ozone.

Our model has a 2-km altitude resolution and extends from the surface to an altitude of 70 km. It is adapted to the latitude at which the instrument is located, i.e., 45°N, and to the day at which the observation is performed. The reaction rates are taken from DeMore *et al.* (1987). For the calculation of the photolysis rate, a plane-parallel approximation is used. The effect of the Earth's sphericity at dawn and dusk upon the optical path of the solar radiation is partly accounted for by using the Chapman function (approximated by Smith and Smith, 1972), rather than the secant of the solar zenith angle. In the spectral region of the O_2 Schumann-Runge bands, the transmission through the atmosphere of solar radiation is derived from the parameterization of Allen and Frederick (1982). At wavelengths less than 300 nm, only the direct flux (attenuated by O_2 and O_3 absorption exclusively, and Rayleigh scattering) is taken into account. At wavelengths beyond 300 nm, where multiple scattering plays a key role, the method of Meier *et al.* (1982) is used with a ground albedo of 0.25, reflecting the partly cloudy conditions encountered at Bordeaux during most of the observations. Mie scattering is ignored. The solar irradiance at the top of the atmosphere is taken from Brasseur and Simon (1981). The formula proposed by Nicolet (1979) is used to approximate the photodissociation coefficient of NO. The temperature profile is taken from Barnett and Corney (1985) for the month corresponding to the observation period. The same temperature profiles are used for the analysis of the ozone spectra measured in Bordeaux. The H_2O profile is assumed to be equal to 4.5 ppmv in the entire middle atmosphere. The system of differential equations

$$\frac{dc_i}{dt} = P_i - L_i c_i, \tag{2}$$

where P_i, L_i and c_i are the production term, the loss coefficient and the concentration of the ith constituent, respectively, is solved using the numerical method of Gear (1971). The order and time step of the method is automatically adjusted to achieve stability and maximize accuracy. The ozone column density is re-evaluated every 10 min for all the altitude levels. Above 35 km altitude, the solution of the chemical system converges after 5 days of integration with differences between the ozone concentrations at two consecutive days being smaller than 1%. We consider this value of 1% as the intrinsic error of the model.

Figure 1a–d shows, as an illustration of the model results, the diurnal variation in the ozone concentration

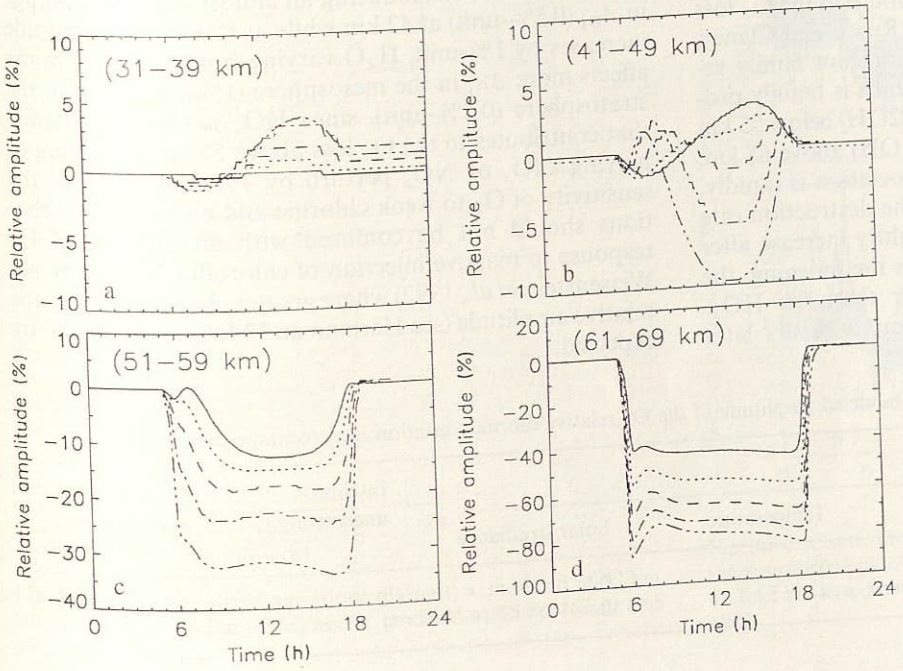

Fig. 1a–d. Ozone diurnal variations relative to its mean night-time value (%-unit) calculated with the 0D model on 15 September at 45°N at: **a** 31 km (*solid*), 33 km (*dot*), 35 km (*dash*), 37 km (*dash dot*) and 39 km (*dash dot dot dot*), **b** 41 km (*solid*), 43 km (*dot*), 45 km (*dash*), 47 km (*dash dot*) and 49 km (*dash dot dot dot*), **c** 51 km (*solid*), 53 km (*dot*), 55 km (*dash*), 57 km (*dash dot*) and 59 km (*dash dot dot dot*), and **d** 61 km (*solid*), 63 km (*dot*), 65 km (*dash*), 67 km (*dash dot*) and 69 km (*dash dot dot dot*)

relative to its mean night-time value at different levels: 31–39 km, 41–49 km, 51–59 km and 61–69 km, respectively (15 September, 45°N). The O_3 diurnal variation is governed by the diurnal variation of the odd oxygen family and the equilibrium balance between O and O_3. This equilibrium resulting from the three main reactions that affect O_3, production ($O + O_2 + M \rightarrow O_3 + M$) and photolytical loss ($O_3 + h\nu \rightarrow O(^1D) + O_2$ and $O_3 + h\nu \rightarrow O + O_2$), is expressed by the ratio

$$\frac{[O]}{[O_3]} = \frac{J_3 + J_3^*}{k_2[M][O_2]}. \quad (3)$$

Knowing that O is almost entirely converted into O_3 during the night, the relative amplitude of the O_3 diurnal variation is proportional to Eq. (3) and increases with height. The odd oxygen, O_x, continuity equation is approximated by

$$\frac{d[O_x]}{dt} \approx 2\{J_2 + J_2^*\}[O_2] - 2k_3[O][O_3] - 2b_3[O][NO_2] - 2d_3[O][ClO] - 2\{a_7[O][HO_2] + a_5[O][OH] + a_{6b}[O_3][HO_2] - a_1[H][O_2][M]\}. \quad (4)$$

The fine structures seen in the daytime portions of the O_3 diurnal variations are caused by the destruction mechanisms induced by the O_x [second term in Eq. (4)], $NO_x = NO + NO_2$ [third term in Eq. (4)], $ClO_x = Cl + ClO$ [fourth term in Eq. (4)] and $HO_x = H + OH + HO_2$ [four last terms in Eq. (4)] families and by the most important reactions in the production channel ($O_2 + h\nu \rightarrow O + O$ and $O_2 + h\nu \rightarrow O(^1D) + O$) [two first terms in Eq. (4)]. During the night, O_3 remains unchanged since the O_3 chemical loss time constant is greater than a day (see Allen *et al.*, 1984), i.e., no more photodissociation, and the O_3 production channel is almost null because of the disappearance of atomic O.

The upper stratosphere is a crossing layer where all the O_x, NO_x, ClO_x and HO_x families contribute to the O_3 loss (see Stolarski and Douglass, 1985, and Rusch and Clancy, 1988). In the mesosphere, the only significant family remaining is HO_x (see Vaughan, 1984) which is mainly produced by the reaction ($H_2O + O(^1D) \rightarrow 2OH$) below 55 km and by the reaction ($H_2O + h\nu \rightarrow H + OH$) above 65 km.

At 61 km (Fig. 1d) the O_2 photodissociation is rapidly, but not instantaneously, balanced by the destruction rate induced by HO_x, permitting O_3 to slightly increase after the deep sunrise fall. At 69 km, early in the morning, the O_2 photodissociation is much greater than the HO_x-induced destruction rate, so the maximum occurs later and its amplitude is greater than at 61 km. This delay in the release of odd hydrogen comes from the replacement of the fast reaction ($H_2O + O(^1D) \rightarrow 2OH$) by the slower reaction ($H_2O + h\nu \rightarrow H + OH$).

2.2 *Ozone sensitivity to parameter changes*

Theoretical O_3 diurnal variations have already been analyzed according to changes in different parameters: surface albedo, H_2O, NO_x and ClO_x, temperature and solar irradiance (see, for instance, Pallister and Tuck, 1983; Vaughan, 1984; Clancy *et al.*, 1987 and Zommerfelds *et al.*, 1989). The aim of this section is, for a given parameter change, to quantify the associated change in the ozone diurnal variation relative to its mean night-time value in order to estimate the overall uncertainty of the modelled O_3 diurnal amplitude.

We define the ozone diurnal amplitude $\Delta_{O_3}(t)$ at time t with respect to its midnight value ($t = 0$) by

$$\Delta_{O_3}(t) = 100 \times \left\{\frac{O_3(t) - O_3(t=0)}{O_3(t=0)}\right\}. \quad (5)$$

We would like to emphasize that the diurnal amplitude of O_3 is in percentage unit (hereafter noted as %-unit) and that, as an example, an increase of 1%-unit in the amplitude of O_3 at 55 km (typically 20%-unit) in fact corresponds to a 5% relative increase. The main interest in choosing the relative amplitude $\Delta_{O_3}(t)$ instead of the absolute amplitude $[O_3(t) - O_3(t=0)]$ is that the analysis is independent of the unit used, i.e., concentration (cm^{-3}) or mixing ratio (ppmv), and changes in some parameters can seriously affect the absolute amplitude (i.e., the well-known temperature dependence of O_3) while slightly disturbing the relative amplitude.

Table 1 lists change (in %-unit) in the diurnal amplitude of ozone calculated at 42 and 55 km depending upon several parameters. Surface albedo has been chosen to vary from 0.0 to 0.5, inducing an almost negligible change in Δ_{O_3} (0.5%-unit) at 42 km while at 55 km, the amplitude increases by 1%-unit. H_2O varying from 4.5 to 6.5 ppmv affects more Δ_{O_3} in the mesosphere (1%-unit) than in the stratosphere (0.2%-unit), since HO_x is the main family that contributes to the O_3 loss above 55 km. Doubling or halving ClO_x or NO_x perturb by 1%-unit Δ_{O_3}, but the sensitivity of O_3 to weak chlorine and nitrogen perturbations should not be confused with an analysis of O_3 response to massive injection of chlorofluorocarbons (see Weisenstein *et al.*, 1992) where greater changes, even in the relative amplitude (see Herman and McQuillan, 1985), are expected.

Table 1. Estimated overall uncertainty in the modeled amplitude of the O_3 relative diurnal variation in percentage unit (%-unit)

Heights /km	Parameters					Intrinsic uncertainty	Overall uncertainty
	Albedo	H_2O	NO_x–ClO_x	Temperature	Solar irradiance		
42	0.5	0.2	1	2	0.5	1	2.5
55	1	1	1	4	2	1	5

The temperature dependence of the ozone concentration has been studied for many years (e.g., Barnett *et al.*, 1975). Fluctuations in temperature field as produced for instance by diurnal and semidiurnal tides (Gille *et al.*, 1991), sudden warmings, gravity waves, etc., can affect the O_3 concentration at a given height dynamically by moving pressure surfaces up and down and photochemically through the temperature and atmospheric density dependence of O_3 at photochemical equilibrium. A 5% perturbation in the temperature vertical profile leads to a 1%-unit and a 4%-unit photochemical change in Δ_{O_3} at 42 and 55 km, respectively; dynamically induced perturbations lead to a 2%-unit change at the two levels. We estimate the uncertainty of O_3 diurnal variations due to temperature changes to be around 2%-unit at 42 km and 4%-unit at 55 km.

Solar irradiances taken from Ackerman (1971), Nicolet (1981) and WMO (1985) produce a 0.5%-unit variation of Δ_{O_3} at 42 km and a 2%-unit at 55 km. To evaluate the overall uncertainty upon the calculated diurnal amplitude, we suppose all the sources of error [induced by the uncertainty upon some parameters in addition to the one intrinsic to the model (1%-unit)] to be uncorrelated. We found that the overall uncertainty is about 2.5%-unit at 42 km and 5%-unit at 55 km.

2.3 Ozone response to the measurement process

Considering the actual and unknown atmospheric O_3 profile, $\varrho(h)$, to be represented by the profile deduced from the 0D model, the ground-based microwave measurement of $\varrho(h)$ in Bordeaux gives in fact two mean O_3 densities $\langle\varrho(h_0)\rangle$ around the layers 42 ± 4.5 and 55 ± 8 km related to $\varrho(h)$ by Eq. (1). Figure 2a shows the amplitudes of the diurnal variations calculated at 42 km and at 42 ± 4.5 km using Eq. (1), while Fig. 2b shows the diurnal amplitude calculated at 55 and 55 ± 8 km using Eq. (1). It is noteworthy that, both in the stratosphere and in the mesosphere, the measurement process affects both the amplitude and the shape of the diurnal variation. Indeed, the amplitude can be reversed from a 4%-unit increase at 3 pm at 42 km to a 2%-unit decrease at 42 ± 4.5 km and can be enlarged from a 20%-unit decrease at 55 km to a 30%-unit decrease around 55 ± 8 km, a signature of the influences of levels higher than the reference heights. Another example of those influences is the slight bump 1.5 h after sunrise calculated at 55 ± 8 km and not visible at 55 km, which is induced by the layers above 60 km (see Fig. 1d).

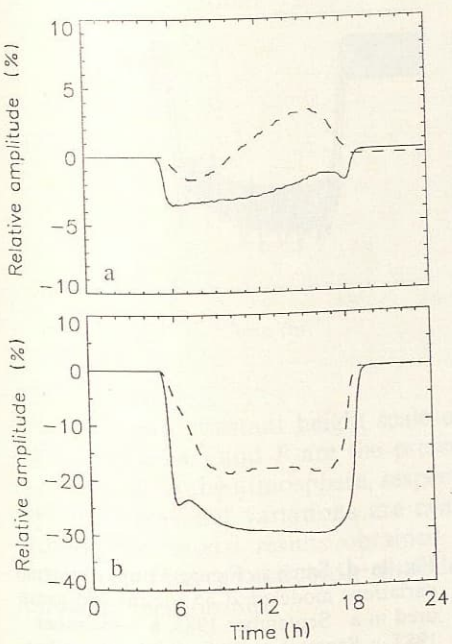

Fig. 2a–b. Ozone diurnal variations (%-unit) **a** modeled at 42 km (*dash*) and 42 ± 4.5 km (*solid*) and **b** modeled at 55 km (*dash*) and 55 ± 8 km (*solid*)

2.4 Comparisons between measured and modeled O_3 diurnal variations

2.4.1 Diurnal variations at 42 ± 4.5 km

Ozone diurnal variations relative to the mean night-time value at 42 ± 4.5 km, only detected in Bordeaux in September 1985, September 1989 and October 1989 (thick lines), are shown in Fig. 3a–c, respectively, together with

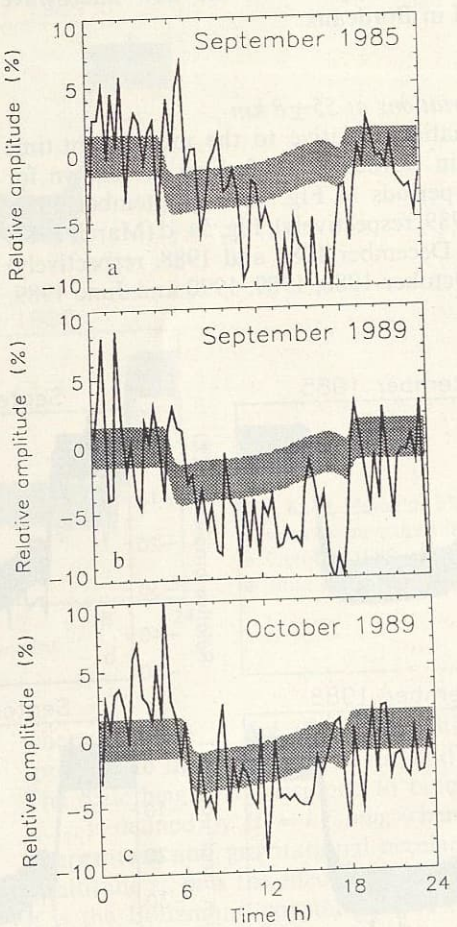

Fig. 3a–c. Ozone diurnal variations (%-unit) modeled according to the appropriate month (*shaded*), and measured in Bordeaux (*solid*) at 42 ± 4.5 km in **a** September 1985, **b** September 1989 and **c** October 1989

the modeled variations (shaded). The shape of all those modeled variations is comparable: a rapid O_3 decrease (2.5%-unit) after sunrise followed by a slight increase throughout the day until sunset. The relative variation measured in September 1989 and October 1989 also shows this early decrease, but with a bigger amplitude, 7 and 5%-unit, respectively. The measured bigger amplitude can be explained by the extreme variability of the night-time measurements that does not enable an optimal determination of the mean night-time value. In September 1985 (Fig. 3a), even if a night-to-day O_3 decrease is measured, the shape and the amplitude of the relative diurnal variation are completely different. Two hours after sunrise, O_3 slowly decreases throughout the day until late in the afternoon when the amplitude is the greatest (8%-unit) and rapidly reaches its night-time value before sunset. In order to attempt an explanation of this discrepancy, we used temperature profiles measured at the Observatoire de Haute Provence (OHP, 600 km from Bordeaux) in September 1985 (A. Hauchecorne, private communication) instead of climatological profiles without noticeable changes in the amplitude and shape of the modeled variation ($\leq$0.5%-unit) which is consistent with the estimations listed in Table 1. An improvement will come from the reduction of night-time variability in the measurement that is supposed to happen with the new microwave receiver installed in Bordeaux.

2.4.2 Diurnal variations at 55±8 km

The diurnal variations relative to the mean night-time value measured in Bordeaux (thick line) are shown for several different periods in Fig. 4a–d (September 1985, 1987, 1988 and 1989, respectively), Fig. 5a–d (March 1987, November 1989, December 1986 and 1988, respectively) and Fig. 6a–d (October 1988, 1989, 1990 and June 1989, respectively). On the same figures, modeled relative diurnal variations, calculated according to the considered month, are plotted (shaded). There is general agreement within 5%-unit between all the modeled and measured diurnal variations except for the October 1988 period when the agreement is within a 10%-unit range. In the October 1988 case, a strong minimum around noon of about 43% is measured, while all the modeled amplitudes are around 33%. This pronounced minimum at noon is quite difficult to interpret in terms of changes in any parameter in the 0D model, since, once again, using temperature profiles measured in OHP slightly reduces the disagreement by around 1%-unit. An interesting feature, commented on in the last section and seen in September 1985 (Fig. 4a), September 1988 (Fig. 4c), September 1989 (Fig. 4d), October 1989 (Fig. 6b) and October 1990 (Fig. 6c), is the O_3 maximum occuring 1.5 h after sunrise and in agreement with all the modeled variations.

3 Ozone seasonal variations

3.1 The 2D model

The seasonal variations of the ozone concentration measured in Bordeaux at 42±4.5 and 55±8 km are now compared with the variations obtained by the 2D chemical/radiative/dynamical model of Brasseur *et al.* (1990). This model provides, as a function of pressure, latitude, and season, the diurnally averaged concentration of nearly 50 chemical species. The 2D model, which has transport equations expressed in the transformed Eulerian framework, is formulated in log-pressure coordinates and provides concentrations at a constant pressure level using the reference altitude z defined by:

$$z = -H_0 \ln\left(\frac{P}{P_0}\right), \tag{6}$$

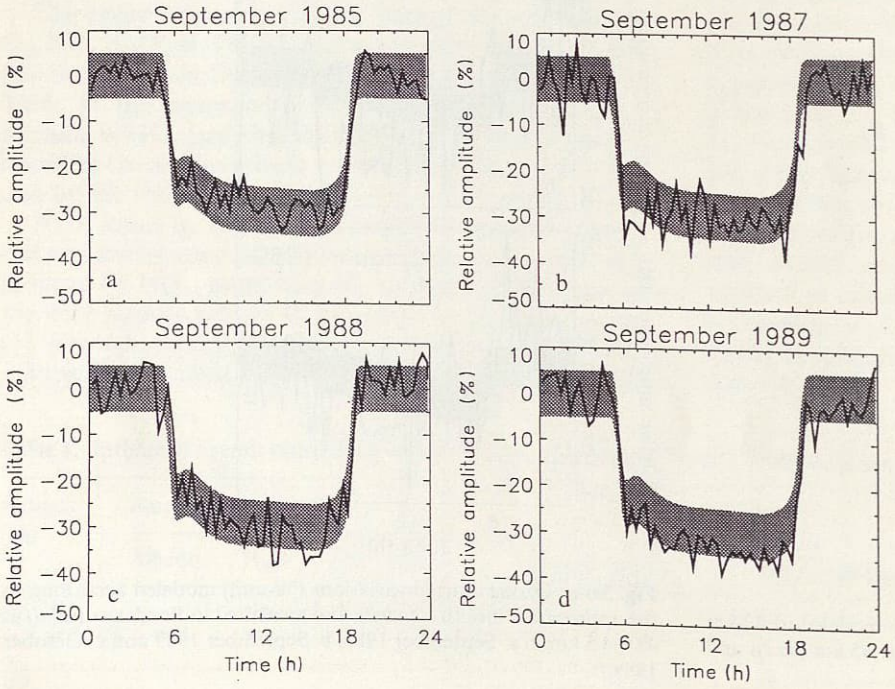

Fig. 4a–d. Same as Figure 3 but for diurnal variations modeled at 55±8 km and measured in **a** September 1985, **b** September 1987, **c** September 1988 and **d** September 1989

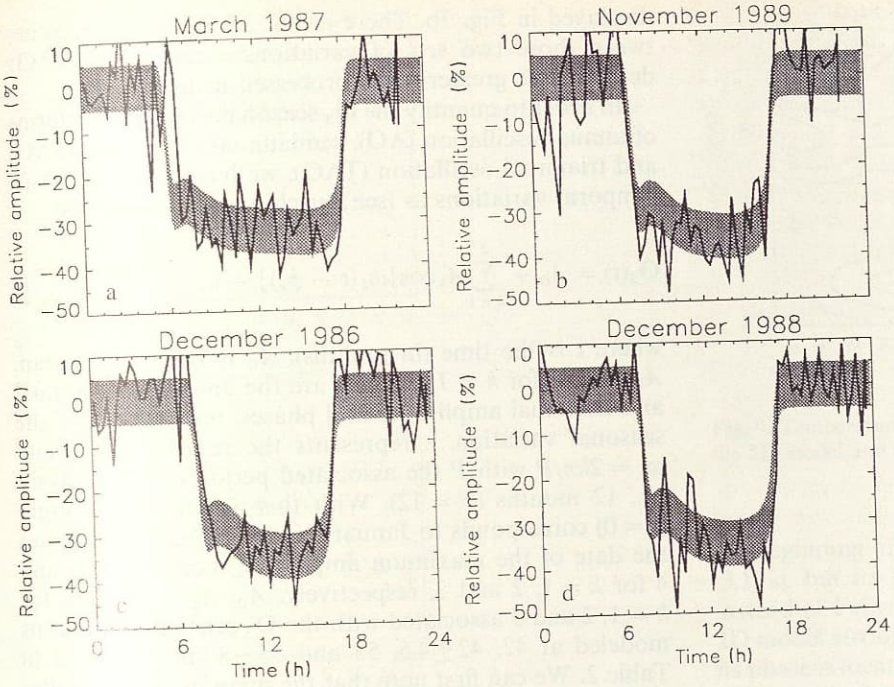

Fig. 5a–d. Same as Fig. 4 but for diurnal variations measured in **a** March 1987, **b** November 1989, **c** December 1986 and **d** December 1988

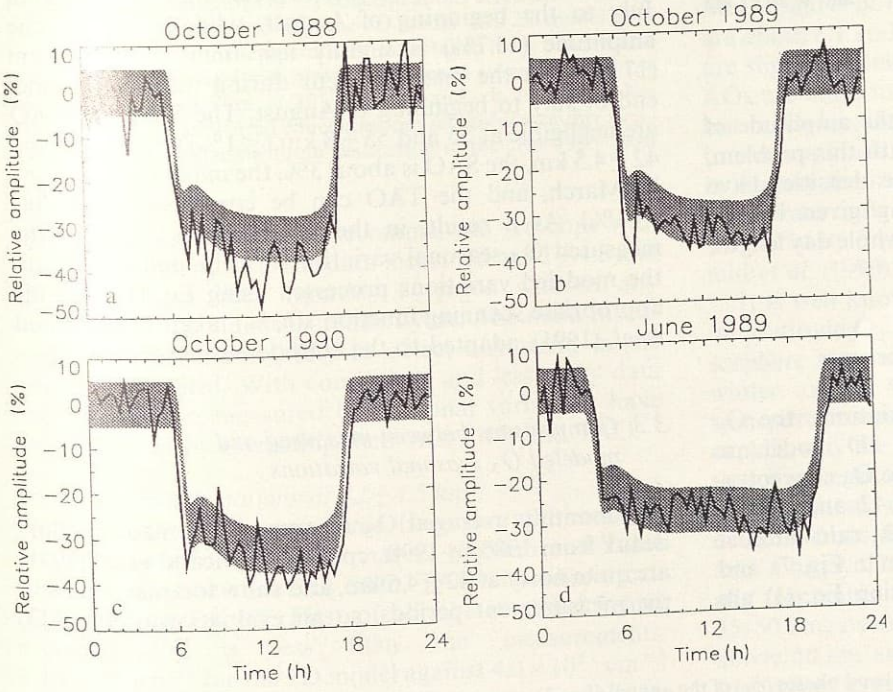

Fig. 6a–d. Same as Fig. 4 but for diurnal variations measured in **a** October 1988, **b** October 1989, **c** October 1990 and **d** June 1989

where H_0 is a constant height scale chosen to be 7 km, P_0(= 1012 mbar) and P are the pressures at the surface ($z_0 = 0$) and in the atmosphere, respectively. Because our measured seasonal variations are evaluated at constant altitude, the model results obtained on pressure levels have been interpolated onto altitude levels, using the following relationship:

$$z_i - z_{i-1} = -H_i \ln\left(\frac{P_i}{P_{i-1}}\right), \tag{7}$$

where z_i and z_{i-1} are the actual altitude layers corresponding to the pressure layers P_i and P_{i-1}, respectively. The scale height H_i, assumed to be constant from z_i to z_{i-1}, is defined by $H_i = kT_i/mg_i$ where T_i and g_i are the temperature and gravitational acceleration, respectively, at altitude z_i, m is the effective molecular mass of air and k is the Boltzmann constant. Since the model provides only diurnally averaged concentration values, comparison with observed data is not straightforward. At 42 km, where the diurnal variation of ozone is less than 5%, the comparison can be easily made, but at 55 km such a direct

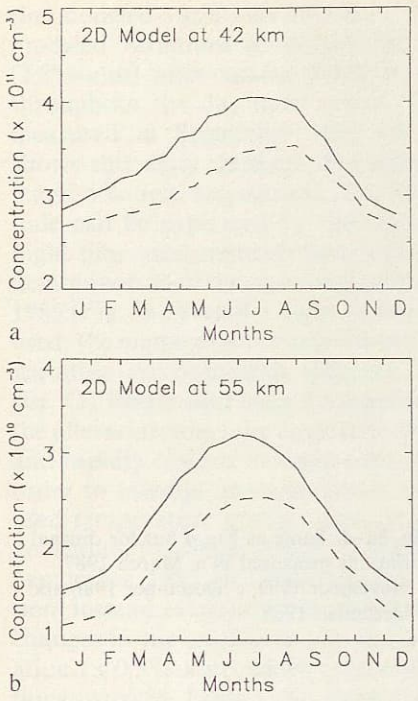

Fig. 7a–b. Modeled seasonal variations of O_3 concentrations **a** at 42 km (*dash*) and 42 ± 4.5 km (*solid*) ($/10^{11}$ cm^{-3}) and **b** at 55 km (*dash*) and 55 ± 8 km (*solid*) ($/10^{10}$ cm^{-3})

comparison is less valuable because of the amplitude of the diurnal variation (20%). To cope with this problem, observed night-time and daytime ozone densities have been weight-averaged, the weight being given by the night-time and daytime lengths over the whole day length, respectively.

3.2 Ozone response to the measurement process

As in the section related to diurnal variations, the O_3 vertical profiles $\varrho(h)$ deduced from the 2D model are processed using Eq. (1) to give $\langle \varrho(h_0) \rangle$, the O_3 concentration at 42 ± 4.5 and 55 ± 8 km for $h_0 = 42$ and 55 km, respectively. The seasonal variations of O_3 calculated at 42 and 42 ± 4.5 km using Eq. (1) are shown in Fig. 7a and those calculated at 55 and 55 ± 8 km using Eq. (1) are displayed in Fig. 7b. There are no strong differences between those two sets of variations except that the O_3 densities are greater when processed using Eq. (1).

In order to quantify the O_3 seasonal variations in terms of annual oscillation (AO), semiannual oscillation (SAO) and triannual oscillation (TAO), we have fitted the $O_3(t)$ temporal variations as (see Rusch and Clancy, 1988):

$$O_3(t) = A_0 + \sum_{k=1}^{3} A_k \cos\{\omega_k (t - \phi_k)\} + \varepsilon, \qquad (8)$$

where t is the time (in months), A_0 is the yearly mean, A_k and ϕ_k for $k = 1, 2$ and 3 are the annual, semiannual and triannual amplitudes and phases, respectively, of the seasonal variation, ε represents the residual error and $\omega_k = 2k\pi/P$ with P the associated period of the analysis, i.e., 12 months ($P = 12$). With this notation, the origin ($t = 0$) corresponds to January and the phase determines the date of the maximum amplitude, modulo 12, 6 and 4 for $k = 1$, 2 and 3, respectively. A_0, A_k/A_0 and ϕ_k for $k = 1$, 2 and 3 associated with the O_3 seasonal variations modeled at 42, 42 ± 4.5, 55 and 55 ± 8 km are listed in Table 2. We can first note that the main modeled oscillation at any level remains the AO: 28.7% amplitude at 55 and 55 ± 8 km with a maximum occurring over the end of July to the beginning of August, while at 42 km, the amplitude (13.7%) is slightly less than at 42 ± 4.5 km (17.1%) but the maxima occur during the same period: end of July to beginning of August. The SAO and TAO are negligible at 55 and 55 ± 8 km ($\leq 1\%$) while at 42 and 42 ± 4.5 km, the SAO is about 3%, the maximum occuring in March, and the TAO can be considered negligible ($\leq 1\%$). As a result, in the following sections, all the measured O_3 seasonal variations will be compared with the modeled variations processed using Eq. (1) with the appropriate scanning function $s(h, h_0)$ taken from Ricaud *et al.* (1991), adapted to the considered month.

3.3 Comparisons between measured and modeled O_3 seasonal variations

The monthly averaged O_3 measurements made in Bordeaux from 1985 to 1990 reported in Ricaud *et al.* (1991) are quite noisy at 42 ± 4.5 km, and show too many gaps in the measurement periods, so an evaluation of the AO,

Table 2. Yearly mean A_0, amplitude ratios (A_k/A_0) and phases (ϕ_k) of the annual ($k = 1$), semiannual ($k = 2$) and triannual ($k = 3$) oscillations calculated by the 2D model, calculated by the 0D model $(O_3)_{eq}$ with 2D model data as input except that the temperature field is taken from Barnett and Corney (1985) and measured in Bordeaux

Seasonal terms	2D model 42	2D model 42 ± 4.5	2D model 55	2D model 55 ± 8	$(O_3)_{eq}$ 42 ± 4.5	$(O_3)_{eq}$ 55 ± 8	Measurements 42 ± 4.5	Measurements 55 ± 8
A_0 (cm^{-3})	3.1×10^{11}	3.4×10^{11}	1.9×10^{10}	2.4×10^{10}	3.5×10^{11}	2.3×10^{10}	4.0×10^{11}	2.3×10^{10}
A_1/A_0 (%)	13.7	17.1	28.7	28.7	13.1	22.0	3.7	13.7
A_2/A_0 (%)	3.0	3.1	1.0	0.5	5.4	5.3	3.5	3.9
A_3/A_0 (%)	0.9	0.7	0.4	0.1	1.3	2.9	3.4	3.7
ϕ_1 (month)	7.4	6.8	7.0	6.6	7.0	5.4	8.3	5.6
ϕ_2 (month)	2.2	2.2	3.3	1.0	0.7	0.4	1.0	0.1
ϕ_3 (month)	1.5	1.4	0.3	0.6	0.4	0.1	1.0	0.8

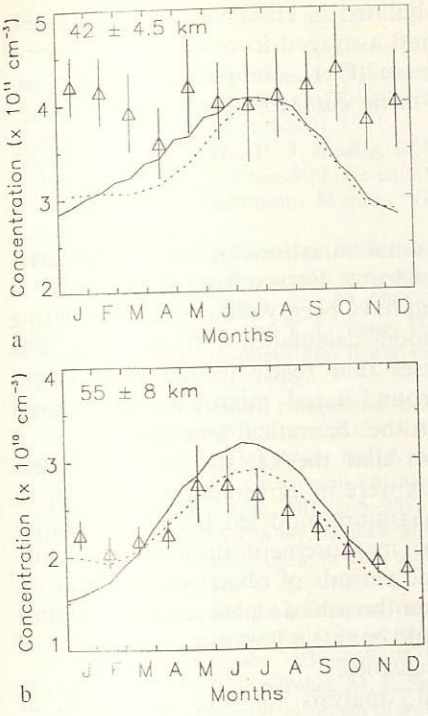

Fig. 8. Seasonal variations of O_3 concentrations calculated with the 2D model (*solid*), calculated with the 0D model with 2D model data as input, except that the temperature field is taken from Barnett and Corney (1985) (*dot*) and measured in Bordeaux (*triangle and error bars*) **a** at 42 ± 4.5 km ($/10^{11}$ cm^{-3}) and **b** at 55 ± 8 km ($/10^{10}$ cm^{-3}). The measured concentrations represent monthly averaged observations made without distinction of the year 1985–1990

SAO and TAO is not to be recommended. To cope with these two difficulties, all the data measured at 42 ± 4.5 and 55 ± 8 km have been monthly averaged without any consideration of the measurement year. The main disadvantage is the impossibility to detect any trend in the measured O_3 field. With continuous and less noisy data over 12 months, measured O_3 seasonal variations have been analyzed by extracting their AO, SAO and TAO.

3.3.1 Seasonal variations at 42 ± 4.5 km

Figure 8a shows the measured (triangle) and modeled (solid line) seasonal variations at 42 ± 4.5 km and Table 2 lists their associated AO, SAO, TAO and phases calculated using Eq. (8). First of all, the modeled yearly averaged O_3 is less than the measurements: 3.4×10^{11} cm^{-3} for the 2D model against 4.0×10^{11} cm^{-3} for the Bordeaux measurements. It is a general issue noticed by several authors (see e.g., WMO, 1985) that modeled O_3 in the stratosphere is deficient by 10–15% compared with measurements. Secondly, the modeled O_3 during the summer period is well-reproduced by the 2D model but the model predicts a winter decrease, while an O_3 winter rise is measured. Table 2 shows that the AO, SAO and TAO measured amplitudes are roughly all about 3.5%: the AO maximum occurring in September, and the SAO and TAO maxima occurring in February. The 2D model mainly overestimates by a factor 4.5 the AO amplitude (17%) and its maximum occurs 1 month earlier than measured: at the end of July as opposed to

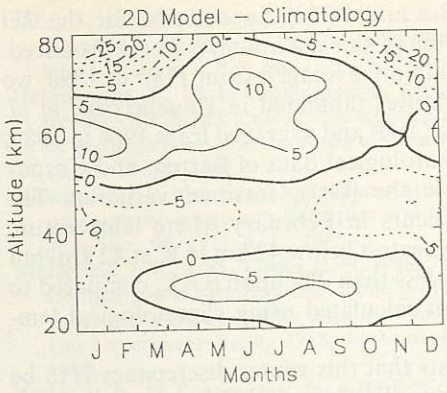

Fig. 9. Temperature difference (Kelvin) between fields generated by the 2D model and climatological data

the beginning of September. The SAO is well-represented (3.1%), but its phase is delayed by 1 month to March instead of February as in the measurements. Finally, the 2D model strongly underestimates the TAO (0.7%), while its phase is located in February. This AO has already been measured by SAGE-II and lidar at 40 and 45 km at Table Mountain (34°N) for the 1988 period and reported in McDermid *et al.* (1990). At 40 km, SAGE-II and lidar AOs are about 8.1 and 7.4%, respectively, while at 45 km, AOs are slightly reduced to 7.6 and 5.6%, respectively. Those AOs are close to the one estimated in Bordeaux (~4%) but much less than the modeled ones (~17%). The maximum amplitude occurs at 40 km in September, at 42 km in August (from Wang *et al.*, 1989) and at 45 km in July. The winter maximum and April minimum have also been measured by SAGE-II and lidar and reported in McDermid *et al.* (1990).

It is well known (see Garcia and Solomon, 1985) that mid-latitude O_3 in the upper stratosphere and lower mesosphere is essentially in photochemical control. But in winter, around 40 km and below, the direct influence of transport processes is certainly not negligible. In order to explain why the AO calculated by the 2D model is larger than the measurements and why it fails to predict a winter O_3 maximum, we have compared the temperature field deduced from the model with field compiled by Barnett and Corney (1985) (see Fig. 9). The 2D model globally generates too low temperatures (5–10 K) within 35–50 km, overestimates the temperature field (5–10 K) above 50 km and between 20 and 35 km, generates too low values in January and February (~5 K), but for the rest of the year modeled temperatures are greater than climatology by about 5 K. If we consider O_3 to be in photochemical equilibrium throughout the year, we can estimate the seasonal variation of $(O_3)_{eq}$, the O_3 at equilibrium calculated using the 0D model with 2D model data as input except that the temperature field is taken from Barnett and Corney (1985). Figure 8a shows the $(O_3)_{eq}$ seasonal variation (dotted line). We can first note that there is no obvious change during the summer and fall periods, while during the January–March period O_3 does not vary at all. The AO, SAO and TAO of $(O_3)_{eq}$, listed Table 2, are now 13.1, 5.4 and 1.3%, respectively,

instead of 17.1, 3.1 and 0.7%, respectively, for the 2D model. However, the winter maximum is not reproduced. Since measured data are averaged from 1985 to 1990, we have used temperatures tabulated in Hauchecorne *et al.* (1991) measured in OHP and averaged from 1984 to 1989, instead of the climatological data of Barnett and Corney (1985), to calculate the $(O_3)_{eq}$ seasonal variation. The maximum effect occurs in February where temperature deviations are the greatest below 42 km (4 K at 42 km) but remains negligible: less than 2% upon $(O_3)_{eq}$ compared to the $(O_3)_{eq}$ variation calculated using climatological temperatures.

Evidence suggests that this winter discrepancy is to be attributed to dynamical processes. The best dynamical candidate remains the propagation of planetary waves with periods ranging from 1 week to 1 month, as already detected in the South of France by Hauchecorne *et al.* (1991). Unfortunately, this 2D model is not able to explicitly reproduce sporadic phenomena that take place during periods of strong wave transience.

3.3.2 Seasonal variations at 55±8 km

The modeled (solid line) and measured (triangle) seasonal variations at 55±8 km can be seen in Fig. 8b. The modeled O_3 yearly average is in very good agreement with the measured one as listed in Table 2: 2.4×10^{10} cm^{-3} for the 2D model and 2.3×10^{10} cm^{-3} for the measurements. The general seasonal shape measured in Bordeaux with summer maximum and winter minimum is globally reproduced by the 2D model, but the modeled summer densities are greater than the measured one, with the reverse in winter. Considering Table 2, we notice that the modeled AO amplitude (28%) is twice the measured one (14%), while its phase is delayed by 1 month from mid-June to mid-July. This maximum AO amplitude occuring during the summer period has already been measured in the northern hemisphere by the SMM instrument in the 53–57 km region from mid-1985 to the beginning of 1989 at 20°N latitude and reported in Aikin *et al.* (1990). They measured an 8% AO amplitude and Allen *et al.* (1984) found that the O_3 density is calculated to be 25% less in winter than in summer at a constant 50 km height. The measured SAO and TAO amplitudes are 3.9 and 3.7%, respectively; these are greater than the modeled ones by 0.5 and 0.1%, respectively. The measured SAO and TAO phases occur at the beginning and end of January, respectively.

At these heights, O_3 is in photochemical equilibrium (see Garcia and Solomon, 1985) and its seasonal variation is exclusively governed by photochemical processes. We have already underlined that the O_3 concentration in the lower mesosphere is highly sensitive to changes in the temperature field. As at 42±4.5 km, we have calculated the seasonal variation of $(O_3)_{eq}$ using the 0D model with 2D model data as input, except that the temperature field is taken from Barnett and Corney (1985). Figure 8b shows the seasonal variation of $(O_3)_{eq}$ (dotted line). The agreement between measured O_3 and modeled $(O_3)_{eq}$ variations is obvious and the modeled $(O_3)_{eq}$ variation lies within the error bars of the measured variation. The modeled AO, SAO and TAO amplitudes and phases listed in Table 2 are much closer to the measured ones. Using the temperature field tabulated in Hauchecorne *et al.* (1991) measured at OHP and averaged from 1984 to 1989 produces a 3% change in $(O_3)_{eq}$ compared to the $(O_3)_{eq}$ variation calculated using climatological temperatures.

4 Conclusions

The diurnal and seasonal variations of ozone concentrations measured in Bordeaux, France from 1985 to 1990 at 42±4.5 and 55±8 km have been validated by comparing with 0D and 2D model calculations, respectively. The measurement processes that relate to the poor height resolution of the ground-based microwave techniques have been included in the theoretical analysis.

It has been shown that the O_3 diurnal amplitudes measured in Bordeaux were in agreement with theory to within 5%. An O_3 maximum modeled 1.5 h after sunrise and attributed to the measurement process is actually measured during some periods of observation. Improvements could come from the use of a new receiver installed in Bordeaux that should enable a lessening in the noise of the retrieved ozone densities.

For the seasonal analysis of O_3 variation, at 42±4.5 km, the 2D model underestimates the yearly averaged ozone concentration compared with the measurements. This is a general issue already mentioned by several authors (see, e.g., WMO, 1985). A double maximum oscillation (~3.5%) is measured in Bordeaux, with an extended maximum in September and a maximum in February associated with a pronounced minimum in April, while the 2D model predicts only a single large maximum (17%) in August and a pronounced minimum in January. Considering O_3 to be in photochemical equilibrium and forcing the temperature field to be as close as possible to climatology, the winter O_3 maximum cannot be reproduced by the 2D model. Evidence suggests then that dynamical transport causes the winter O_3 maximum by propagation of planetary waves, phenomena which are not explicitly reproduced by the 2D model.

At 55±8 km, the modeled yearly averaged O_3 concentration is in very good agreement with the measured yearly average. The maximum is modeled to occur in summer and the minimum in winter, but the measured variations, while, showing a summer maximum, also present a slight maximum in January-February. At these heights, ozone is exclusively in photochemical control and disagreements between the measured and modeled seasonal variations are attributed to temperature fields generated by the 2D model that differ from climatological or measured averaged data.

Acknowledgements. We would like to thank A. Hauchecorne for providing us temperature data measured in OHP. Ph. Ricaud is indebted to C. Granier at NCAR for useful discussions and R. Harwood at Edinburgh University for his support. The computations were performed at NCAR, Boulder, Colo., USA; LPCE, Orléans, France; Department of Meteorology, Edinburgh, Great Britain; and Bordeaux Observatory, France. The National Center for Atmospheric Research is sponsored by the National Science Foundation. Topical Editor P. Mascart thanks M. Chipperfield and G. Vaughan for their help in evaluating this paper.

References

Ackerman, M., Ultraviolet solar radiation related to mesospheric processes, in *Mesospheric models and related experiments*, Ed. G. Fiocco, D. Reidel, Dordrecht, 1971.

Aikin, A. C., W. Henze, D. J. Kendig, R. Nakatsuka, and H. J. P. Smith, Variations of mesospheric equatorial ozone as observed by the Solar Maximum Mission, *Geophys. Res. Lett.*, **17,** 299–302, 1990.

Allen., M., and J. E. Frederick, Effective photodissociation cross sections for molecular oxygen and nitric oxide in the Schumann-Runge bands, *J. Atmos. Sci.*, **39,** 2066–2075, 1982.

Allen, M., J. I. Lunine, and Y. L. Yung, The vertical distribution of ozone in the mesosphere and lower thermosphere, *J. Geophys. Res.*, **89,** 4841–4872, 1984.

Backus, G., and F. Gilbert, Uniqueness in the inversion of inaccurate gross Earth data, *Phil. Trans. R. Soc. London*, **266,** 123–192, 1970.

Barnett, J. J., J. T. Houghton, and J. A. Pyle, The temperature dependence of the ozone concentration near the stratopause, *Q. J. R. Meteorol. Soc.*, **101,** 245–257, 1975.

Barnett, J. J., and M. Corney, Middle atmosphere reference model derived from satellite data, *Middle Atmosphere Program*, Handbook for MAP, **16,** 47–85, 1985.

Bevilacqua, R. M., and J. J. Olivero, Vertical resolution of middle atmospheric measurements by ground-based microwave telemetry, *J. Geophys. Res.*, **93,** 9463–9475, 1988.

Bevilacqua, R. M., D. F. Strobel, M. E. Summers, J. J. Olivero, and M. Allen, The seasonal variation of water vapor and ozone in the upper mesosphere: Implications for vertical transport and ozone photochemistry, *J. Geophys. Res.*, **95,** 883–893, 1990.

Brasseur, G., and P. C. Simon, Stratospheric chemical and thermal response to long-term variability in solar UV irradiance, *J. Geophys. Res.*, **86,** 7343, 1981.

Brasseur, G., and S. Solomon, Aeronomy of the Middle Atmosphere: chemistry and physics in the stratosphere and mesosphere, D. Reidel, Hingham, Mass., 1984.

Brasseur, G., M. H. Hitchman, S. Walters, M. Dymek, E. Falise, and M. Pirre, An interactive chemical dynamical radiative two-dimensional model of the middle atmosphere, *J. Geophys. Res.*, **95,** 5639–5655, 1990.

Brillet, J., A theoretical study of ozone measurements made with ground-based microwave sensors, *J. Geophys. Res.*, **94,** 12833–12850, 1989.

Clancy, R. T., D. W. Rusch, R. J. Thomas, M. Allen, and R. S. Eckman, Model ozone photochemistry on the basis of Solar Mesosphere Explorer mesospheric observations, *J. Geophys. Res.*, **92,** 3067–3080, 1987.

Connor, B. J., J. W. Barrett, A. Parrish, P. M. Solomon, R. L. de Zafra, and M. Jamarillo, Ozone over McMurdo station, Antarctica, austral spring 1986: altitude profiles for the middle and upper atmosphere, *J. Geophys. Res.*, **92,** 13221–13230, 1987.

DeMore, W. B., M. J. Molina, S. P. Sander, D. M. Golden, R. F. Hampson, M. J. Kurylo, C. J. Howard, and A. R. Ravishankara, Chemical kinetics and photochemical data for use in stratospheric modeling, *Publ.* **87-41,** Jet Propul. Lab., Calif., 1987.

De Zafra, R. L., M. Jamarillo, J. Barrett, L. K. Emmons, P. M. Solomon, and A. Parrish, New observations of a large concentration of ClO in the springtime lower stratosphere over Antarctica and its implications for ozone-depleting chemistry, *J. Geophys. Res.*, **94,** 11423–11428, 1989.

Garcia, R. R., and S. Solomon, The effect of breaking gravity waves on the dynamics and chemical structure of the middle atmosphere, *J. Geophys. Res.*, **90,** 3850–3868, 1985.

Gear, C. W., Numerical initial value problems in ordinary differential equations, Prentice Hall, Englewood Cliffs, N.J., 1971.

Gille, S., A. Hauchecorne, and M. L. Chanin, Semidiurnal and diurnal tide effects in the middle atmosphere as seen by Rayleigh lidar, *J. Geophys. Res.*, **96,** 7579–7587, 1991.

Hauchecorne, A., M. L. Chanin, and P. Keckhut, Climatology and trends of the middle atmospheric temperature (33–87 km) as seen by Rayleigh lidar over the South of France, *J. Geophys. Res.*, **96,** 15,297–15,309, 1991.

Herman, J. G., and C. J. McQuillan, Atmospheric chlorine and stratospheric ozone non-linearities and trend detection, *J. Geophys. Res.*, **90,** 5721–5732, 1985.

McDermid, I. C., S. M., Godin, P.-H. Wang, and M. P. McCormick, Comparison of stratospheric ozone profiles and their seasonal variations as measured by lidar and Stratospheric Aerosol and Gas Experiment during 1988, *J. Geophys. Res.*, **95,** 5605–5612, 1990.

Meier, R. R., D. E. Anderson, Jr., and M. Nicolet, Radiation field in the troposphere and stratosphere from 240–1000 nm. I. General analysis, *Planet. Space Sci.*, **30,** 923–933, 1982.

Nicolet, M., Photodissociation of nitric oxide in the mesosphere and stratosphere: simplified numerical relations for atmosphere model calculation, *Geophys. Res. Lett.*, **6,** 866, 1979.

Nicolet, M., The solar spectral irradiance and its action in the atmospheric photodissociation processes, *Planet. Space Sci.*, **29,** 951–974, 1981.

Pallister, R. C., and A. F. Tuck, The diurnal variation of ozone in the upper stratosphere as a test of photochemical theory, *Q. J. R. Meteorol. Soc.*, **109,** 271–284, 1983.

Ricaud, Ph., J. Brillet, J. de La Noë, and J.-P. Parisot, Diurnal and seasonal variations of strato-mesospheric ozone: analysis of ground-based microwave measurements in Bordeaux, France, *J. Geophys. Res.*, **96,** 18617–18629, 1991.

Rusch, D. W., and R. T. Clancy, Trends in atmospheric ozone: conflicts between models and SBUV data, *J. Geophys. Res.*, **93,** 8431–8437, 1988.

Smith III, F. L., and C. Smith, Numerical evaluation of Chapman's grazing incidence integral $Ch(R, \chi)$, *J. Geophys. Res.*, **77,** 3592–3597, 1972.

Solomon, P. M., R. de Zafra, A. Parrish, and J. W. Barrett, Diurnal variation of stratospheric chlorine monoxide: a critical test of chlorine chemistry in the ozone layer, *Science*, **224,** 1210–1214, 1984.

Stolarski, R. S., and A. R. Douglass, Parameterization of the photochemistry of stratospheric ozone including catalytic loss processes, *J. Geophys. Res.*, **90,** 10,709–10,718, 1985.

Vaughan, G., Mesospheric ozone: theory and observation, *Q. J. R. Meteorol. Sco.*, **110,** 239–260, 1984.

Wang, P.-H., M. P. McCormick, L. R. McMaster, S. Schaffner, and G. E. Woodbury, Time-periodic variations in stratospheric ozone from satellite observations, in *Proc. Quadrennial Ozone Symposium*, Eds. R. Bojkov and P. Fabian, 247–250, A. Deepak, Hampton, Va., 1989.

Weisenstein, D. K., M. K. W. Ko, and N.-D. Sze, The chlorine budget of the present-day atmosphere: a modeling study, *J. Geophys. Res.*, **97,** 2547–2559, 1992.

Wilson, W. J., and P. R. Schwartz, Diurnal variations of mesospheric ozone using millimeter wave measurements, *J. Geophys. Res.*, **86,** 7385–7388, 1981.

World Meteorological Organization, Atmospheric ozone, An assessment of our understanding of the processes controlling its present distribution and change, *Global Ozone Res. Monit. Proj. Rep.*, **16,** 1985.

Zommerfelds, W. C., K. Künzi, M. E. Summers, R. M. Bevilacqua, D.F. Strobel, M. Allen, and W. J. Sawchuck, Diurnal variations of mesospheric ozone obtained by ground-based microwave radiometry, *J. Geophys. Res.*, **94,** 12,819–12,832, 1989.